

Anisotropic Tolman V Solutions by Decoupling Approach in $f(R, T^2)$ Gravity

M. Sharif ^{*} and Shazmeena Iltaf [†]

Department of Mathematics, University of the Punjab,
Quaid-e-Azam Campus, Lahore-54590, Pakistan.

Abstract

This paper investigates the behavior of anisotropic static spheres that are constructed by employing a minimal geometric deformation in the framework of $f(R, T^2)$ gravity ($T^2 = T_{\zeta\nu}T^{\zeta\nu}$, R is the Ricci scalar and $T_{\zeta\nu}$ is the energy-momentum tensor). We consider a spherical setup with two sources: seed and additional. It is assumed that the seed source is isotropic whereas the new source is responsible for inducing anisotropy. We deform the g_{rr} component to split the field equations into two sets. The first array corresponds to the isotropic solution whereas the second set contains the effect of the anisotropic source. The system related to isotropic source is determined by the metric potentials of Tolman V solution while three solutions of the second set are constructed corresponding to three different constraints. The physical acceptability of all solutions is checked through energy conditions by employing the radius and mass of PSR J1614-2230 star. We also examine the stability, mass, compactness and redshift of the obtained solutions. We conclude that first two solutions satisfy the viability and stability criteria only for small values of the decoupling parameter while third solution is stable for its all possible values.

^{*}msharif.math@pu.edu.pk

[†]shazmeenailtaf39@gmail.com

Keywords: Gravitational decoupling; Energy-momentum squared gravity; Exact solutions.

PACS: 04.50.Kd; 04.40.-b; 04.20.Jb

1 Introduction

The well-structured universe is composed of celestial bodies whose physical behavior and arrangement help in comprehending the evolution of the universe. In this regard, general relativity (GR) plays an important role in extending our knowledge regarding the mechanism of cosmos as well as the interior of heavenly bodies. The solutions of field equations in GR explain different physical phenomena such as planetary dynamics, black holes and evolution of the universe. However, the non-linearity of the field equations creates a problem in the formation of physically viable exact solutions. Moreover, the extreme central density in compact stellar objects indicates the presence of anisotropic pressure. Compact stars have dense cores and their density exceeds the nuclear density, therefore, pressure must be anisotropic inside them [1]. The existence of interacting nuclear matter in dense compact objects gives rise to the generation of anisotropy [2]. The inclusion of anisotropy further complicates the extraction of solutions that effectively describe the structure and mechanism of celestial bodies. Many researchers have dedicated their efforts towards devising techniques that aid in the formulation of well-behaved solutions.

In this regard, Mak and Harko [3] calculated anisotropic solutions of the field equations and observed that the decreasing behavior of matter density and pressure, supports the interior of astronomical objects. Gleiser and Dev [4] analyzed the stability of the self-gravitating system in the presence of anisotropic pressure and found that the physical structure of a star is significantly affected by pressure anisotropy. Sharma and Maharaj [5] obtained the exact anisotropic solutions to the field equations for a linear equation of state. The graphical behavior of different parameters (mass, energy density and pressure gradient) have been observed for anisotropic stars by introducing conformal motion [6]. Kalam et al. [7] constructed an anisotropic solution in the framework of Krori and Barua (KB) metric. The different possibilities have been discussed for the existence of anisotropic compact star in higher-dimensional spacetime [8]. Maurya et al. [9] computed charged anisotropic solutions representing compact stars and investigated various physical prop-

erties (energy conditions, stability and anisotropy).

Recently, the approach of gravitational decoupling through a minimal geometric deformation (MGD) was introduced which helps in finding new analytical solutions in astrophysics as well as cosmology. Ovalle [10] first introduced the decoupling technique in the context of Randall-Sundrum braneworld. This technique adds a new gravitational source coupled to the energy-momentum tensor of the seed matter distribution through a dimensionless parameter. In this approach, deformation is applied only in the radial metric component while the temporal metric function remains unaltered. Consequently, non-linear field equations are split into two sets that exclusively correspond to seed or additional source. The solution of each set is evaluated separately and combined afterward to obtain a new solution. The technique of decoupling has been generally used to extend the domain of isotropic solutions by incorporating an anisotropic source.

Ovalle [11] developed anisotropic solutions through this technique by using Tolman IV ansatz as a solution of the set associated with the isotropic source. Hairy black hole solutions were obtained by incorporating different characteristics of the additional gravitational source [12]. Anisotropic solutions analogous to Durgapal-Fuloria [13], Buchdahl [14] and KB [15] spacetimes have also been constructed through the MGD scheme. Morales and Tello-Ortiz [16] studied the charged anisotropic Heintzmann solution and checked the graphical behavior of matter variables for different stars. The effect of anisotropy on the Korkina-Orlyanskii [17] and Tolman VII [18] perfect fluid solutions has been observed through decoupling technique. Casadio et al. [19] applied the gravitational decoupling method to develop anisotropic solutions by applying the condition of vanishing complexity factor. Sharif and Sadiq [20] analyzed the effect of charge on decoupled solutions and concluded that stability enhances in the presence of charge. Zubair and Azmat [21] computed an anisotropic solution by specifying the system corresponding to the isotropic source through Tolman V solution. Rincón et al. [22] analyzed the features of (2+1)-dimensional black hole using the MGD approach. Contreras et al. [23] applied decoupling through MGD on the exterior Schwarzschild solution to formulate new solutions. The gravitational decoupling method has also been adopted to generate axially symmetric black hole solutions [24]. Recently, Carrasco-Hidalgo and Contreras [25] formulated a new model for ultra-compact anisotropic star through the MGD method and used the zero complexity condition to close the system of field equations.

Cosmologists initially believed that the attractive nature of gravitational

force will ultimately lead to the decelerated expansion of the cosmos. However, on the contrary, different observations confirm its current accelerated expansion. Supernova type Ia has a known brightness, that can be used as standard candles to determine the luminosity distance of galaxies. The distance-redshift relation is the most essential approach for measuring the history of cosmic expansion. One uses observations of supernova type Ia to calculate luminosity distances at various redshifts and the other uses measurements of baryon acoustic oscillations to determine angular diameter distances at several redshifts. The non-linear feature of luminosity distance versus red-shift fits with the accelerated expansion of the universe. In the light of cosmological observations, it is necessary to look for a new approach that is compatible with our findings. In order to explain the present accelerated expansion of the universe, physicists coined the term dark energy to explain the mysterious force whose negative pressure is causing the galaxies to drift apart with acceleration. Many efforts have been done by several researchers to uncover this mysterious force. In this regard, the cosmological constant is considered as the best candidate to explain the mysterious aspects of dark energy, but it has two major problems involving the fine tuning and coincidence problem.

Modified theories have successfully played the role of alternatives to the dark energy. Such theories are formed by adding the higher-order curvature invariants in the geometric part of the Einstein-Hilbert (EH) action. In this regard, the $f(R)$ gravity is obtained by replacing the Ricci scalar (R) with the generic function $f(R)$ in the geometric part of EH action [26]. The $f(R)$ gravity has been further generalized by introducing coupling between the matter sector and the geometrical quantities leading to $f(R, L_m)$ theory (L_m is matter Lagrangian) [27]. The $f(R, \mathbf{T})$ gravity ($\mathbf{T} = T_{\zeta\nu}g^{\zeta\nu}$) is one of such modifications obtained by replacing the matter lagrangian with the trace of energy-momentum tensor in $f(R, L_m)$ theory [28]. A generic theory in which matter and geometry are non-minimally coupled was introduced in [29], referred to as $f(R, \mathbf{T}, R_{\zeta\nu}T^{\zeta\nu})$, where $R_{\zeta\nu}$ is the Ricci tensor and $T^{\zeta\nu}$ is the energy-momentum tensor. Sharif and Waseem [30] constructed the charged anisotropic solutions and observed that the presence of charge provides more stable behavior in $f(R)$ theory. Anisotropic solutions by decoupling technique have been constructed by using isotropic KB solution in this theory [31]. Plenty of work has been done to obtain viable and stable solutions through decoupling technique in $f(R, \mathbf{T})$ and $f(R)$ theories [32]-[37]. Various viable and stable solutions have been obtained through decoupling

technique in $f(R, \mathbf{T}, R_{\zeta\nu}T^{\zeta\nu})$ [38, 39] framework.

The Big Bang theory is still the most generally recognized cosmological model that explains evolution of the cosmos. The theory specifies how the cosmos evolved from a high-temperature state, a high density as well as a variety of well-known observations such as cosmic microwave background radiations, large-scale structures, and the abundance of light elements. According to the Big Bang theory, all the matter in the cosmos exploded from a singularity. The occurrence of singularities is the major issue in GR. The existence of a singularity at the beginning of the cosmos is explained at high energy levels where GR is not viable. In this regard, $f(R, T^2)$ (where R is the Ricci scalar and $T^2 = T^{\zeta\nu}T_{\zeta\nu}$) gravity is considered as a favourable theory which resolves the singularity problem. In 2014, Katirci and Kavuk [40] developed this theory by adding a non-linear term $T^2 = T^{\zeta\nu}T_{\zeta\nu}$ in the geometric part of the EH action and discussed the cosmological applications for the model $f(R, T^2) = R + \beta T^2$, where β is the real-valued coupling parameter. This theory is also referred to as the energy-momentum squared (EMSG) gravity. Such matter-geometry coupling explains different eras of the universe as well as the rotation curves of galaxies. Faraji et al. [41] used Friedmann-Lemaitre-Robertson-Walker (FLRW) metric to observe the effect of coupling parameter and found that the range $(0, 2.1 \times 10^5]$ provides observationally viable inflationary model. Several remarkable results have also been obtained by using the Kuchowicz metric in this scenario [42]. A gravitational model acts only as an alternative to the mysterious dark energy. These models also explain the cosmic expansion. In the study of the early universe, this theory supports a regular bounce, i.e., a cosmos with finite maximum energy density and a minimal scale factor. It can resolve the singularity problem with classical prescription.

Using a specific model of EMSG, Board and Barrow [43] computed exact solutions to discuss different scenarios related to isotropic distribution, the existence of singularities as well as evolution of the cosmos. Nari and Roshan [44] compared the results of GR and EMSG while describing compact stars. The compactness of a neutron star has been computed for different values of the coupling parameter lying within the range $(-10^{-38} \text{cm}^3/\text{erg}, 10^{-37} \text{cm}^3/\text{erg})$ [45]. Bahamonde et al. [46] discussed the phase space and stability analysis for different models in EMSG. The viability of isotropic cosmos has also been analyzed in this theory by using flat FLRW metric [47]. Sharif and Gul [48] constructed various cosmological as well as astrophysical solutions via different techniques and discussed their viability and stability.

Recently, Sharif and Naz [49] have computed gravastar structure in the perspective of curvature-matter coupled theory and concluded that the physical features of gravastar follow the increasing trend against the thickness of the shell.

In this paper, we decouple the field equations through a deformation in the radial metric function to generate anisotropic analogs of Tolman V in the background of EMSG. The paper is organized according to the following arrangement. In section 2, we derive the field equations for a static sphere filled with two sources which are decoupled through the MGD scheme in section 3. We develop three anisotropic solutions and use the junction conditions to specify the unknown constraints in section 4. Section 5 discusses the physical behavior, viability and stability of all the solutions graphically. We conclude our results in section 6.

2 $f(R, T^2)$ Field Equations

In this section, we construct the field equations in the framework of EMSG. The complete action for this theory in the presence of additional source is

$$S = \frac{1}{2\kappa^2} \int f(R, T^2) \sqrt{-g} d^4x + \int L_m \sqrt{-g} d^4x + \alpha \int L_\Phi \sqrt{-g} d^4x, \quad (1)$$

where $\kappa^2 = \frac{8\pi G}{c^4}$, R , L_Φ and L_m denote the coupling constant, Ricci scalar, Lagrangian densities of new source ($\Phi_{\zeta\nu}$) and matter distribution, respectively. Further, g is the determinant of the metric tensor and α is the decoupling parameter. For the sake of simplicity, we take the gravitational constant (G) and speed of light (c) as 1 and thus $\kappa^2 = 8\pi$. This action represents that this theory has additional degrees of freedom. As a result of the extra force and a matter-dominated era, it is believed that some important results will be gained to analyze the present cosmic problems in this gravity. Variation of the action (1) with respect to the metric tensor leads to the following field equations

$$R_{\zeta\nu} f_R + g_{\zeta\nu} \square f_R - \nabla_\zeta \nabla_\nu f_R - \frac{1}{2} g_{\zeta\nu} f = 8\pi (T_{\zeta\nu} + \alpha \Phi_{\zeta\nu}) - \Theta_{\zeta\nu} f_{T^2}, \quad (2)$$

where \square is the d'Alembertian operator (which is defined as $\square = \nabla_\zeta \nabla^\zeta$), $f_{T^2} = \frac{\partial f}{\partial T^2}$, $f_R = \frac{\partial f}{\partial R}$ and

$$T_{\zeta\nu} = g_{\zeta\nu} L_m - 2 \frac{\partial L_m}{\partial g^{\zeta\nu}}. \quad (3)$$

and

$$\Theta_{\zeta\nu} = \frac{\partial T^2}{\partial g^{\zeta\nu}} = -2L_m(T_{\zeta\nu} - \frac{1}{2}g_{\zeta\nu}T) - 4\frac{\partial^2 L_m}{\partial g^{\zeta\nu}\partial g^{\alpha\beta}}T^{\alpha\beta} - TT_{\zeta\nu} + 2T_{\zeta}^{\beta}T_{\nu\beta}. \quad (4)$$

Different choices of the matter Lagrangian for a perfect fluid have been analyzed in literature. These include $L_m = \pm P$ [50], $L_m = T$ [51] and $L_m = \pm\rho$ [52]. The sign depends on the signatures of the chosen metric. Here we take metric signatures $(+, -, -, -)$ along with $L_m = -P$, which is one of the probable Lagrangian for a perfect fluid mentioned in the literature [53, 54]. The energy-momentum tensor for perfect fluid is

$$T_{\zeta\nu} = (\rho + P)U_{\zeta}U_{\nu} - g_{\zeta\nu}P, \quad (5)$$

where U_{ζ} , ρ and P represent the four-velocity, energy density and pressure, respectively. Inserting $L_m = -P$ in Eq.(4) yields

$$\Theta_{\zeta\nu} = (3P^2 + \rho^2 + 4P\rho)U_{\zeta}U_{\nu}. \quad (6)$$

By rearranging Eq.(2), we obtain

$$G_{\zeta\nu} = \frac{1}{f_R} \left(8\pi(T_{\zeta\nu}^{(m)} + \alpha\Phi_{\zeta\nu}) - g_{\zeta\nu}\square f_R + \nabla_{\zeta}\nabla_{\nu}f_R - \Theta_{\zeta\nu}f_{T^2} + \frac{1}{2}g_{\zeta\nu}(f - Rf_R) \right), \quad (7)$$

where $G_{\zeta\nu} = R_{\zeta\nu} - \frac{1}{2}Rg_{\zeta\nu}$ is the Einstein tensor.

To describe the spherical structure of self-gravitating objects, we consider the static line element

$$ds^2 = e^{\xi}dt^2 - e^{\eta}dr^2 - r^2d\theta^2 - r^2\sin^2\theta d\phi^2, \quad (8)$$

where the metric potentials (ξ, η) depend on the radial coordinate only. We consider the model $f(R, T^2) = R + \beta T^2$ to make our results meaningful. Using Eqs.(5) and (6) in (7), the field equations corresponding to the above model become

$$8\pi(\tilde{\rho} + \alpha\Phi_0^0) = e^{-\eta}\left(\frac{\eta'}{r} - \frac{1}{r^2}\right) + \frac{1}{r^2}, \quad (9)$$

$$8\pi(\tilde{P} - \alpha\Phi_1^1) = e^{-\eta}\left(\frac{\xi'}{r} + \frac{1}{r^2}\right) - \frac{1}{r^2}, \quad (10)$$

$$8\pi(\tilde{P} - \alpha\Phi_2^2) = \frac{e^{-\eta}}{4}\left(2\xi'' - \frac{2\eta'}{r} + \frac{2\xi'}{r} - \xi'\eta' + \xi'^2\right), \quad (11)$$

where

$$\tilde{\rho} = \rho - \frac{1}{16\pi}(\rho^2 + 3P^2 + 8\rho P)\beta, \quad (12)$$

$$\tilde{P} = P - \frac{1}{16\pi}(\rho^2 + 3P^2)\beta. \quad (13)$$

Here, prime represents the derivative with respect to the radial coordinate and β is the model parameter having dimensions of L^2 . The energy-momentum conservation law does not hold in EMSG as the covariant derivative of Eq.(7) takes the following form

$$\begin{aligned} \nabla^\zeta(\Theta_{\zeta\nu}f_{T^2}) - \frac{1}{2}g_{\zeta\nu}\nabla^\zeta f &= \tilde{P}' + \frac{\xi'}{2}(\tilde{\rho} + \tilde{P}) + \alpha \left(\frac{\xi'}{2}(\Phi_0^0 - \Phi_1^1) \right. \\ &\quad \left. + \frac{2}{r}(\Phi_2^2 - \Phi_1^1) - \Phi_1^{1'} \right). \end{aligned} \quad (14)$$

The field equations are non-linear differential equations containing seven unknown functions: the matter variables ($\tilde{\rho}$, \tilde{P}), the metric potentials (ξ , η) and the extra source components (Φ_0^0 , Φ_1^1 , Φ_2^2). The effective energy density, effective radial and tangential pressures are, respectively, defined as

$$\bar{\rho} = \tilde{\rho} + \alpha\Phi_0^0, \quad (15)$$

$$\bar{P}_r = \tilde{P} - \alpha\Phi_1^1, \quad (16)$$

$$\bar{P}_t = \tilde{P} - \alpha\Phi_2^2. \quad (17)$$

Moreover, the anisotropy generated by $\Phi_{\zeta\nu}$ in the self-gravitating object has the following form for $\Phi_1^1 \neq \Phi_2^2$

$$\Delta = \bar{P}_t - \bar{P}_r = \alpha(\Phi_1^1 - \Phi_2^2). \quad (18)$$

If $\beta \rightarrow 0$, the field equations in $f(R, T^2)$ gravity will reduce to GR.

3 Gravitational Decoupling

In this section, we use the method of gravitational decoupling through MGD to solve the system of field equations. In order to incorporate the impact of the decoupling parameter in the perfect fluid distribution, we consider the following geometric modifications

$$\zeta \rightarrow \xi = \zeta + \alpha s(r), \quad (19)$$

$$\nu \rightarrow e^{-\eta} = \nu + \alpha h(r), \quad (20)$$

where s and h represent the deformations in temporal and radial components, respectively. As we are using the MGD approach, we perform geometric deformation only in the radial component while the temporal function remains unaltered, i.e., $s = 0$. We obtain two sets of equations by using Eq.(20) in the set of field equations. The first set of equations is obtained for $\alpha = 0$ and is given as

$$8\pi\tilde{\rho} = \frac{1}{r^2} - \left(\frac{\nu}{r^2} + \frac{\nu'}{r}\right) = 8\pi\rho - \frac{1}{2}(\rho^2 + 3P^2 + 8\rho P)\beta, \quad (21)$$

$$8\pi\tilde{P} = -\frac{1}{r^2} + \frac{\nu}{r}\left(\frac{1}{r} + \xi'\right) = 8\pi P - \frac{1}{2}(\rho^2 + 3P^2)\beta, \quad (22)$$

$$8\pi\tilde{P} = \frac{\nu}{2r}(\xi''r + \frac{\xi'^2r}{2} + \xi') + \frac{\nu'}{2}\left(\frac{\xi'}{2} + \frac{1}{r}\right) = 8\pi P - \frac{1}{2}(\rho^2 + 3P^2)\beta, \quad (23)$$

whereas the second set describing the anisotropic source is given as

$$8\pi\Phi_0^0 = -\frac{h'}{r} - \frac{h}{r^2}, \quad (24)$$

$$8\pi\Phi_1^1 = -\frac{h}{r}\left(\frac{1}{r} + \xi'\right), \quad (25)$$

$$8\pi\Phi_2^2 = -\frac{2h}{r}\left(\xi'' + \frac{\xi'^2}{2} + \frac{\xi'}{r}\right) - \frac{h'}{2r}\left(\frac{\xi'r}{2} + 1\right). \quad (26)$$

The energy-momentum conservation equations for both scenarios take the following forms

$$\nabla^\zeta(\Theta_{\zeta\nu}f_{T^2}) - \frac{1}{2}g_{\zeta\nu}\nabla^\zeta f = \tilde{P}' + \frac{\eta'}{2}(\tilde{\rho} + \tilde{P}), \quad (27)$$

$$\Phi_1^{1'} - \frac{\eta'}{2}(\Phi_0^0 - \Phi_1^1) - \frac{2}{r}(\Phi_2^2 - \Phi_1^1) = 0. \quad (28)$$

Simultaneously solving Eqs.(21)-(23) provides complicated expressions of energy density and pressure. To simplify calculations, we apply the following relation

$$P = \rho = \frac{m}{V}, \quad (29)$$

where $V = \frac{4}{3}\pi r^3$ is the volume of sphere. Using this equation, $\tilde{\rho}$ and \tilde{P} can be written in the form of mass as

$$\tilde{\rho} = \frac{3m(16\pi^2r^3 - 9m\beta)}{64\pi^3r^6}, \quad (30)$$

$$\tilde{P} = \frac{48m\pi^2 r^3 - 9m^2\beta}{64\pi^3 r^6}. \quad (31)$$

The effective energy density and pressure of the isotropic source is described by Eqs.(30) and (31), respectively.

4 Anisotropic Solutions

Tolman [55] presented eight perfect fluid solutions of the field equations in the background of a static spherical spacetime. We choose the components of Tolman V solution to solve Eqs.(21)-(23). Tolman V is a natural solution used for investigating the fluid spheres with infinite density and pressure at the center. This solution has been previously used to specify the metric components related to the seed source [21]. The metric coefficients of Tolman V solution are

$$e^{\xi(r)} = C^2 r^{2n}, \quad (32)$$

$$e^{\eta(r)} = \nu^{-1} = \frac{1 + 2n - n^2}{1 - (1 + 2n - n^2)\left(\frac{r}{R}\right)^W}, \quad (33)$$

where $W = \frac{2(1+2n-n^2)}{1+n}$. The values of the constants appearing in the metric potentials of Tolman V solution are determined by using the matching conditions [56]. These conditions play an important role in the study of stellar geometry as they provide a smooth junction between the exterior and interior regions at the boundary ($\Sigma : r = \mathcal{R}$) of the star. The essential conditions are given as

$$(ds_+^2)_\Sigma = (ds_-^2)_\Sigma, \quad \bar{P}_r(\mathcal{R}) = 0, \quad (34)$$

which imply that radial pressure drops to zero at the boundary which is essential for the stability of a star. We use Schwarzschild metric to describe the exterior geometry as

$$ds_+^2 = - \left(\frac{2M}{\mathcal{R}} - 1 \right) dt^2 + \left(\frac{2M}{\mathcal{R}} - 1 \right)^{-1} dr^2 - r^2 d\theta^2 - r^2 \sin^2 \theta d\phi^2, \quad (35)$$

where M represents the mass of compact object. The constants are evaluated by using the junction conditions as

$$C^2 = \frac{M}{n\mathcal{R}^{2n+1}}, \quad (36)$$

$$n = \frac{M}{\mathcal{R} - 2M}, \quad (37)$$

$$\left(\frac{\mathcal{R}}{F}\right)^W = \frac{M(M\mathcal{R} - 2M^2)}{\mathcal{R}(\mathcal{R}^2 - 2M\mathcal{R} - M^2)}. \quad (38)$$

We have three field equations and four unknowns in the second set comprising additional source. To minimize the number of unknowns ($h(r)$, Φ_0^0 , Φ_1^1 , Φ_2^2), we need a some constraint. For this purpose, we use mimic constraints as well as an equation of state on components of $\Phi_{\zeta\nu}$ to obtain three viable solutions.

4.1 Solution I

To find the values of unknowns, we apply a condition on Φ_0^0 . For this motive, we use the constraint [31]

$$\Phi_0^0 = \bar{\rho}. \quad (39)$$

By using Eqs.(21), (24), (32) and (33), we obtain the following expression of the deformation function,

$$h = -\frac{8\pi \left(n^2 - 2n + (n^2 - 2n - 1) \left(\frac{r}{F}\right)^W \right)}{(n^2 - 2n - 1)} + \frac{d}{r},$$

where d is an integration constant. If $r = 0$, then the above result diverge. So, we assume $d = 0$ and obtain the reduced form of the deformation function as

$$h = -\frac{8\pi \left(n^2 - 2n + (n^2 - 2n - 1) \left(\frac{r}{F}\right)^W \right)}{(n^2 - 2n - 1)}. \quad (40)$$

Using Eq.(40), we calculate the values of the matter variables as

$$\begin{aligned} \bar{\rho} &= \frac{\left(\left(\frac{r}{F}\right)^W (1 + W)(n^2 - 1 - 2n) - 2n + n^2 \right) \alpha}{(n^2 - 1 - 2n)r^2} \\ &+ \frac{3m(16\pi^2 r^3 - 9m\beta)}{64\pi^3 r^6}, \end{aligned} \quad (41)$$

$$\begin{aligned}\bar{P}_r &= -\frac{(1+2n)\left(\left(\frac{r}{F}\right)^W(n^2-2n-1)+n^2-2n\right)\alpha}{(n^2-2n-1)r^2} \\ &+ \frac{48m\pi^2r^3-9m^2\beta}{64\pi^3r^6},\end{aligned}\quad (42)$$

$$\begin{aligned}\bar{P}_t &= \frac{32r^4\left(\frac{r}{F}\right)^W W(1+3n+n^2-n^3)-\left(\frac{r}{F}\right)^W(64r^4n^4-128r^4n^3)\alpha}{64r^6(n^2-2n-1)} \\ &+ \frac{64r^4n^2\left(\frac{r}{F}\right)^W-64r^4n^4+128r^4n^3}{64r^6(n^2-2n-1)}\alpha + \frac{48m\pi^2r^3-9m^2\beta}{64r^6\pi^3}.\end{aligned}\quad (43)$$

We graphically analyze the physical features for PSR J1614-2230 star with mass $1.97M_\odot$ (M_\odot is solar mass) and radius $11.29km$. The model parameter in this case can be positive or negative. However, we do not get viable and stable results for its positive values and thus, we use negative values of β to obtain acceptable solutions. Moreover, the value of the model parameter is fixed as -0.1 for $\alpha = 0.1, 0.21$. The energy density and pressures of a viable model attain maximum values near $r = 0$ and decrease monotonically towards the surface. Moreover, positive anisotropy, obtained for $P_t > P_r$, implies the existence of an outward repulsive force. Figure 1 indicates that the physical parameters and anisotropy attain the maximum values near the center and remain finite throughout for the assumed values of parameters. Moreover, the radial pressure drops to zero as $r \rightarrow \mathcal{R}$.

4.2 Solution II

In this section, we apply a condition on Φ_1^1 to determine the deformation function h . For this purpose, we use the mimic constraint [12]

$$\Phi_1^1 = \tilde{P}. \quad (44)$$

Using Eqs.(22) and (25) alongwith the metric potential of Tolman V solution, the deformation function is evaluated as

$$h(r) = \frac{8\pi\left(n^2+(2n^3-3n^2-4n-1)\left(\frac{r}{F}\right)^W\right)}{(1+2n)(n^2-2n-1)}. \quad (45)$$

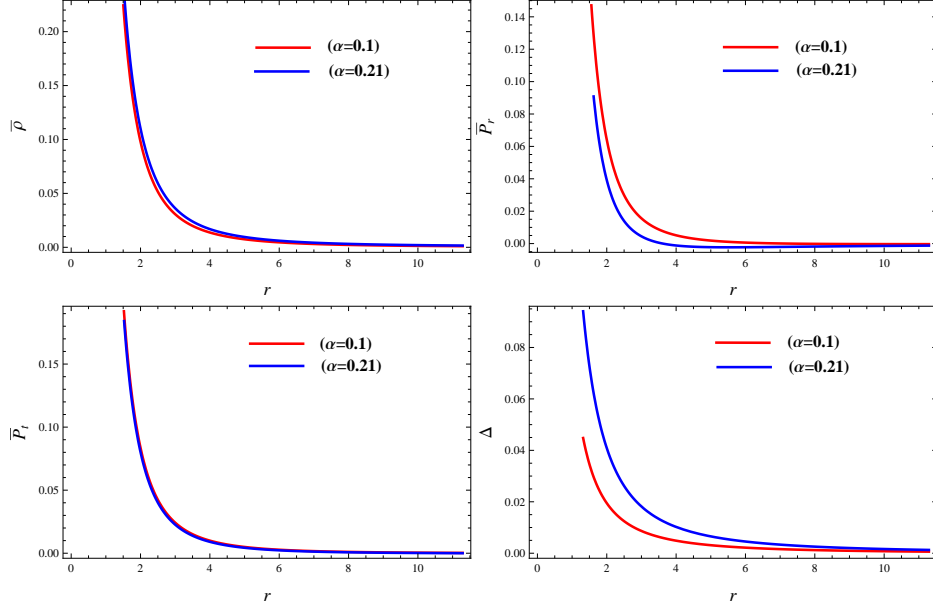


Figure 1: Behavior of energy density, radial/tangential pressures and anisotropy of the first solution.

Equations (33) and (45) provide the minimally deformed Tolman V solution. Employing Eq.(45), we develop the expressions of effective parameters as

$$\begin{aligned} \bar{\rho} &= \frac{\left(\frac{r}{F}\right)^W (1+W)(1+4n+3n^2-2n^3) - n^2}{(1+2n)(n^2-2n-1)r^2} \alpha \\ &+ \frac{3m(16\pi^2 r^3 - 9m\beta)}{64\pi^3 r^6}, \end{aligned} \quad (46)$$

$$\bar{P}_r = \frac{\left(\frac{r}{F}\right)^W (1+4n+3n^2-2n^3) - n^2}{(n^2-2n-1)r^2} \alpha + \frac{48m\pi^2 r^3 - 9m^2\beta}{64\pi^3 r^6}, \quad (47)$$

$$\begin{aligned} \bar{P}_t &= -\frac{32r^4 \left(\frac{r}{F}\right)^W (2n^2+8n^3+6n^4-4n^5) + (5n+1+7n^2) \left(\frac{r}{F}\right)^W W}{64r^6(1+2n)(n^2-1-2n)} \alpha \\ &- \frac{(2n^4-n^3)W \left(\frac{r}{F}\right)^W}{64r^6(2n+1)(n^2-1-2n)} \alpha - \frac{2n^4}{64r^6(1+2n)(n^2-2n-1)} \alpha \\ &+ \frac{48m\pi^2 r^3 - 9m^2\beta}{64r^6\pi^3}. \end{aligned} \quad (48)$$

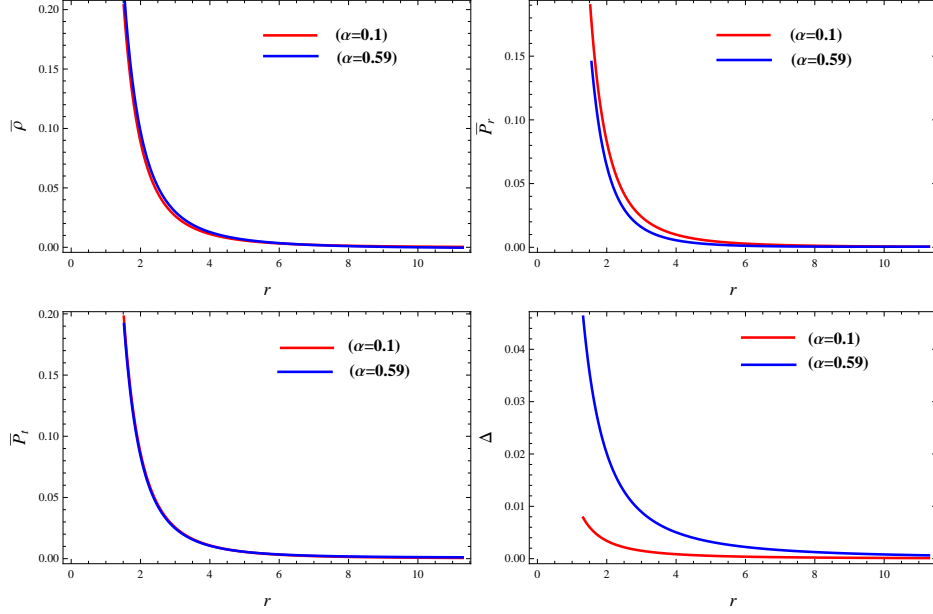


Figure 2: Behavior of energy density, radial/tangential pressures and anisotropy of the second solution.

We consider the same value of β by considering the same star for $\alpha = 0.1, 0.59$. The effective energy density and effective pressures of a viable model attain maximum values near the center and decrease monotonically towards the boundary. Figure 2 indicates that the effective parameters attain the maximum values near the core and decrease towards the boundary. Figure 2 also describes the positive anisotropy.

4.3 Solution III

In order to formulate the third anisotropic solution, we apply a linear equation of state on $\Phi_{\zeta\nu}$ as [57]

$$\Phi_0^0 = \Phi_1^1, \quad (49)$$

which leads to

$$h(r) = r^{2n} A, \quad (50)$$

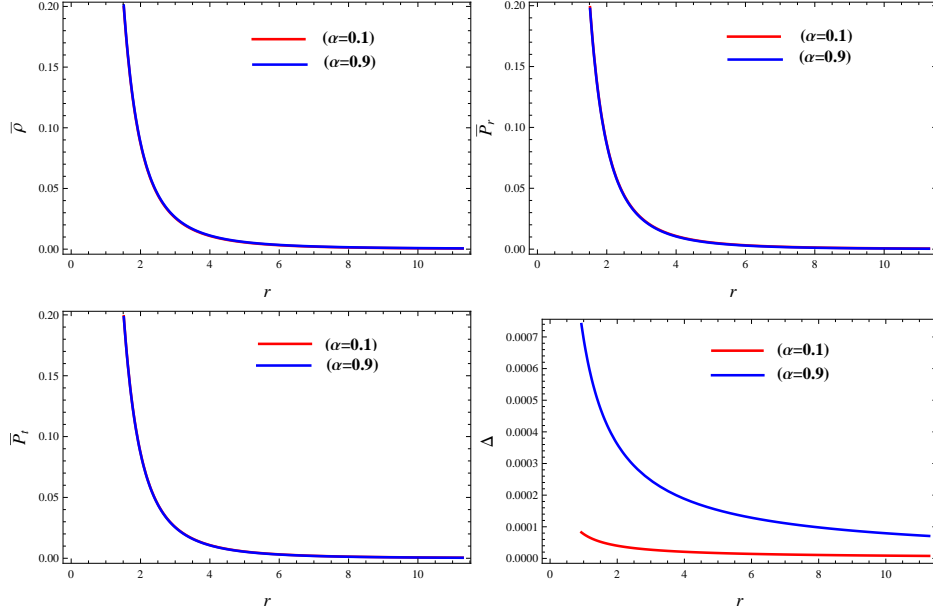


Figure 3: Behavior of energy density, radial/tangential pressures and anisotropy of the third solution.

where A is an integration constant. By using Eq.(50), we find the anisotropic solution as

$$\bar{\rho} = \frac{48m\pi^2 r^3 - 8(1+2n)\pi^2 r^{4+2n} A\alpha - 27m^2\beta}{64\pi^3 r^6}, \quad (51)$$

$$\bar{P}_r = \frac{48m\pi^2 r^3 + 8(1+2n)\pi^2 r^{4+2n} A\alpha - 9m^2\beta}{64\pi^3 r^6}, \quad (52)$$

$$\bar{P}_t = \frac{48m\pi^2 r^3 + 8n(1+2n)\pi^2 r^{4+2n} A\alpha - 9m^2\beta}{64\pi^3 r^6}. \quad (53)$$

We consider the same values of M , \mathcal{R} and β as in solution I and II. Moreover, A is fixed as -0.02 while we take two values of the decoupling parameter as 0.1 and 0.9 . From Figure 3, it is observed that $\bar{\rho}$, \bar{P}_r , \bar{P}_t and anisotropy have the maximum values near the core of the star and decrease continuously as r increases.

5 Graphical Analysis

We check the essential physical characteristics of the anisotropic solutions using energy conditions, stability criteria, mass, compactness and redshift parameter.

5.1 Energy Conditions

Energy constraints are used to check the existence of ordinary matter as well as physical viability of the resulting solutions. These constraints are classified into weak, strong, null and dominant energy conditions. For anisotropic matter distribution, these constraints are defined as

$$\begin{aligned}
 WEC : \quad & \bar{\rho} + \bar{P}_r \geq 0, \quad \bar{\rho} \geq 0, \quad \bar{\rho} + \bar{P}_t \geq 0, \\
 SEC : \quad & \bar{\rho} + \bar{P}_t \geq 0, \quad \bar{\rho} + \bar{P}_r \geq 0, \quad \bar{\rho} + \bar{P}_r + 2\bar{P}_t \geq 0, \\
 NEC : \quad & \bar{\rho} + \bar{P}_r \geq 0, \quad \bar{\rho} + \bar{P}_t \geq 0, \\
 DEC : \quad & \bar{\rho} - |\bar{P}_r| \geq 0, \quad \bar{\rho} - |\bar{P}_t| \geq 0.
 \end{aligned}$$

The energy conditions show the same trend as the matter variables and all solutions are consistent with the criteria of physically acceptable solutions for the assumed values of parameters.

5.2 Causality Condition

A compact structure is stable if it satisfies the condition that the speed of light exceeds the speed of sound traveling through its medium [58]. Thus, the radial and tangential components of sound velocity should, respectively, satisfy the inequalities

$$0 < v_r^2 < 1, \quad 0 < v_t^2 < 1, \quad (54)$$

where $v_r^2 = \frac{d\bar{P}_r}{d\bar{\rho}}$ and $v_t^2 = \frac{d\bar{P}_t}{d\bar{\rho}}$. The speed of sound in radial direction violates the causality limit for $\alpha = 0.21$ and 0.59 corresponding to solution I and II, respectively. The speed of sound in tangential direction corresponding to first, second and third anisotropic model satisfies the stability limit as shown in Figures 4-6. Herrera's cracking approach [59] is another procedure to check the stability of models. The solutions are stable if the speed of sound in the radial and tangential directions satisfy the limit $0 < |v_t^2 - v_r^2| < 1$. The anisotropic Tolman V solutions satisfy this limit as shown in Figures 4-6.

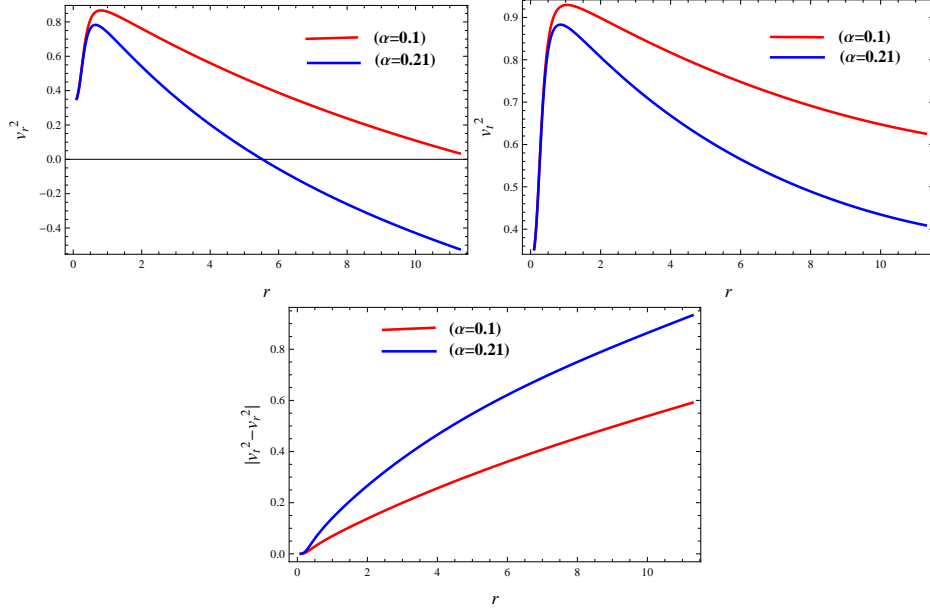


Figure 4: Plots of causality condition and Herrera's cracking approach of solution I.

5.3 Redshift and Compactness

The effective mass of self-gravitating object for anisotropic spherically symmetric fluid distribution is given as

$$m(r) = 4\pi \int_0^r \bar{\rho} r^2 dr. \quad (55)$$

It is very difficult to find effective mass by using the above relation in the modified theories. Therefore, we use an effective way to find the mass using the metric components as

$$m(r) = \frac{r(1 - e^{-\eta(r)})}{2}. \quad (56)$$

The mass of the above three solutions increases as r increases as shown in Figures 7-9. The compactness of the stellar system is determined by using the relation

$$\mu(r) = \frac{m(r)}{r}. \quad (57)$$

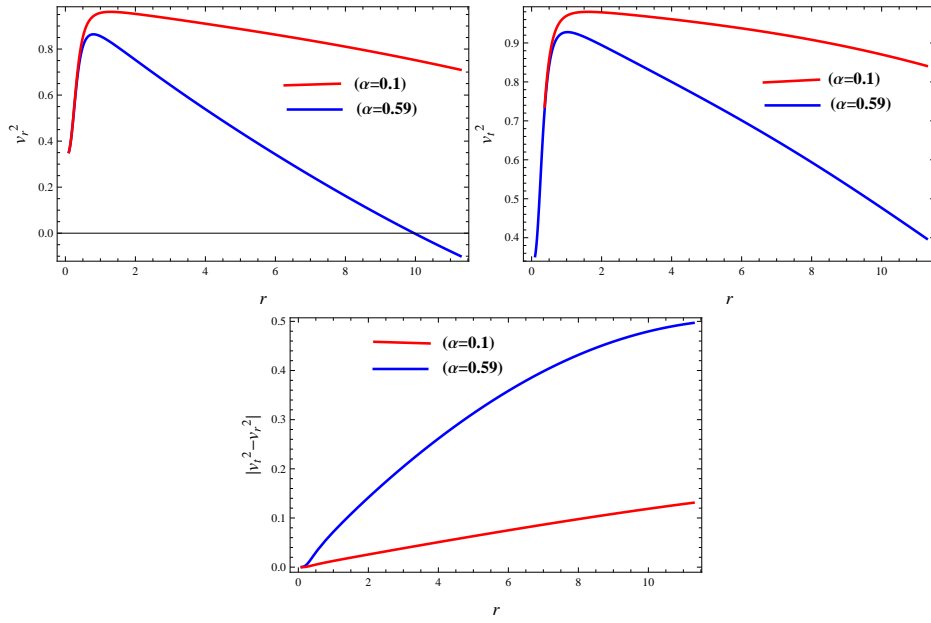


Figure 5: Plots of causality condition and Herrera's cracking approach of solution II.

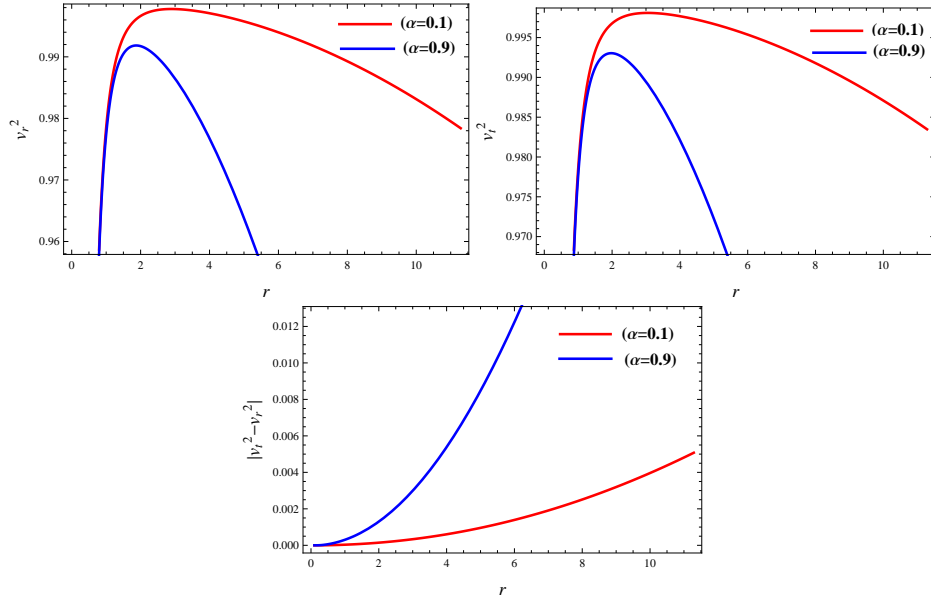


Figure 6: Plots of causality condition and Herrera's cracking approach of solution III.

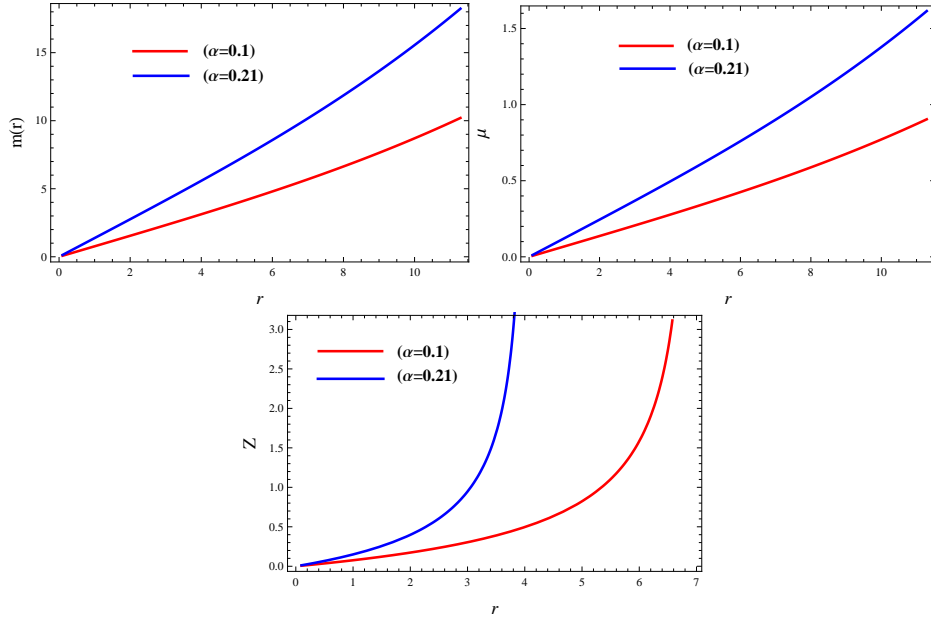


Figure 7: Behavior of mass, compactness and redshift of solution I.

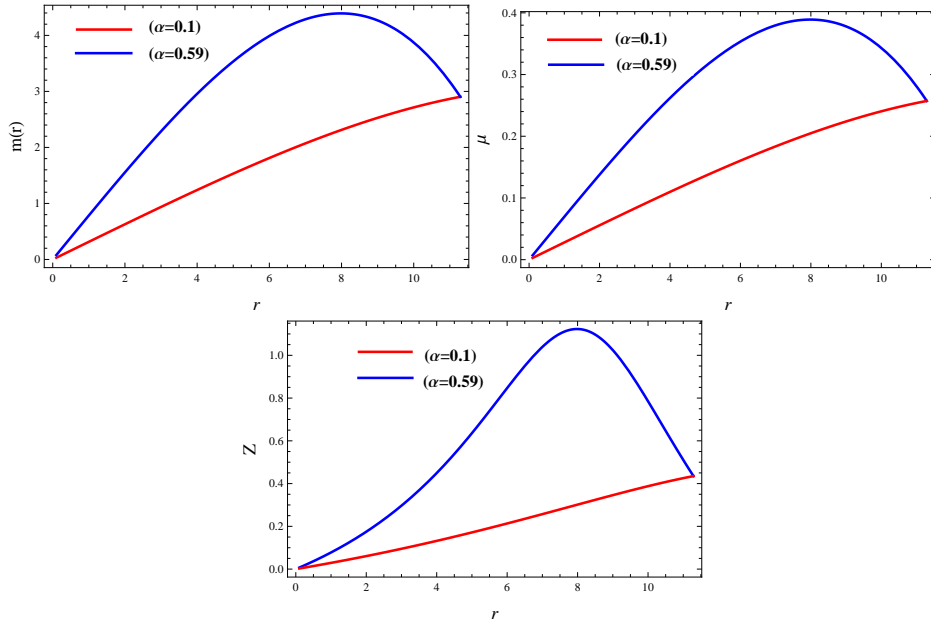


Figure 8: Plots of mass, compactness and redshift of solution II.

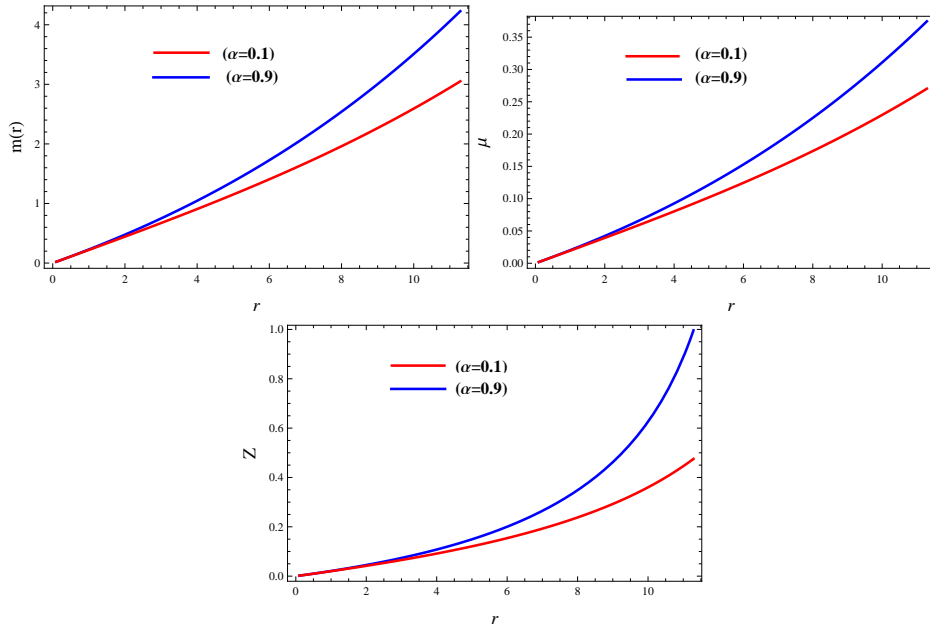


Figure 9: Behavior of mass, compactness and redshift of solution III.

The upper limit of compactness for anisotropic fluid ($\frac{M}{R} < \frac{4}{9}$) was measured by Buchdahl [60]. The compactness parameter of solution I does not attain the corresponding limit (Figure 7). Second and third anisotropic Tolman V solutions agree with this limit (Figures 8 and 9). The surface redshift of self-gravitating body measures the increment in wavelength of electromagnetic radiation due to the gravitational pull of that body. The redshift parameter is defined as

$$Z = -1 + \frac{1}{\sqrt{1 - 2\mu}}, \quad (58)$$

whose maximum value for anisotropic solution is $Z \leq 4.77$ [61]. The graph of redshift parameter increases as r increases for all the anisotropic solutions, as shown in Figures 7-9. For solutions II and III, the values of redshift parameter remains below the value 4.77 for the chosen values of the model and decoupling parameters. The redshift parameter corresponding to the solution I does not attain the corresponding limit.

6 Concluding Remarks

Gravitational decoupling through the MGD method has been extensively used to obtain well-behaved models of the self-gravitating system. In this paper, we have constructed anisotropic solutions using this approach in the context of EMSG. For this reason, we have added a new anisotropic source alongside the isotropic energy-momentum tensor. The field equations containing anisotropic as well as seed matter distributions have been decoupled into two sets through a radial transformation. One set consists of the standard field equations of EMSG while the other corresponds to the anisotropic source. To check the effectiveness of this technique, we have described the first array by considering the metric potentials of the isotropic Tolman V solution along with the model $f(R, T^2) = R + \beta T^2$. We have applied the junction conditions by taking the Schwarzschild metric as exterior space-time to find the values of constants appearing in the solution. The physical viability of all solutions is analyzed through the behavior of effective parameters, anisotropy and energy constraints for some specific values of decoupling and model parameters. We have also checked the stability of the extended solutions through causality condition and Herrera's cracking approach. The behavior of mass, compactness and redshift of anisotropic extensions has also been investigated.

For the first solution, we have applied the constraint $\Phi_0^0 = \tilde{\rho}$, whereas the second and third solutions have been constructed by using a constraint $\Phi_1^1 = \tilde{P}$ and a linear equation of state relating Φ_0^0 and Φ_1^1 , respectively. We have graphically examined the new anisotropic solutions by utilizing the radius and mass of PSR J1614-2230 star. Further, the values of parameters are fixed as $\beta = -0.1$ with $\alpha = 0.1, 0.21, \alpha = 0.1, 59$ and $\alpha = 0.1, 0.9$ for solutions I, II and III, respectively. For all solutions, the effective energy density, radial and tangential pressures attain the maximum values near the core of star and decrease continuously towards its boundary. Furthermore, all the obtained solutions are viable as they satisfy all the energy conditions for the chosen values of the parameters. The speed of sound in radial direction does not satisfy the stability limit for $\alpha = 0.21$ and 0.59 for solution I and II, respectively whereas the solution III satisfies this criteria for $\alpha = 0.1, 0.9$. Moreover, the Herrera's cracking approach lies within the limit $0 < |v_t^2 - v_r^2| < 1$ for all anisotropic solutions. The mass, compactness and redshift show increasing behavior for above three solutions and the limits $\frac{M}{R} < \frac{4}{9}$ and $Z \leq 4.77$ are fulfilled only by solutions II and III. We conclude that solution

III is physically viable and stable in the framework of EMSG for all values of the decoupling parameter, whereas solutions I and II are viable only for $\alpha \leq 0.21$ and $\alpha \leq 0.59$, respectively.

Appendix A

The energy conditions corresponding to solution I are

$$\begin{aligned}
\bar{\rho} &= \frac{\left(n^2 - 2n + \left(\frac{r}{F}\right)^W (1+W)(n^2 - 1 - 2n) \right) \alpha}{(n^2 - 1 - 2n)r^2} \\
&+ \frac{3m(16\pi^2 r^3 - 9m\beta)}{64\pi^3 r^6}, \\
\bar{\rho} + \bar{P}_r &= \frac{\left(\left(\frac{r}{F}\right)^W (1+W)(n^2 - 1 - 2n) - 2n + n^2 \right) \alpha}{(n^2 - 1 - 2n)r^2} \\
&- \frac{(1+2n) \left(n^2 - 2n + \left(\frac{r}{F}\right)^W (n^2 - 1 - 2n) \right) \alpha}{(n^2 - 1 - 2n)r^2} \\
&+ \frac{48m\pi^2 r^3 - 9m^2\beta}{64\pi^3 r^6} + \frac{3m(16\pi^2 r^3 - 9m\beta)}{64\pi^3 r^6}, \\
\bar{\rho} + \bar{P}_t &= \frac{32r^4 \left(\frac{r}{F}\right)^W W(1+3n+n^2-n^3) - \left(\frac{r}{F}\right)^W (64r^4 n^4 - 128r^4 n^3)}{64r^6(n^2 - 2n - 1)} \alpha \\
&+ \frac{64r^4 n^2 \left(\frac{r}{F}\right)^W - 64r^4 n^4 + 128r^4 n^3}{64r^6(n^2 - 2n - 1)} \alpha + \frac{48m\pi^2 r^3 - 9m^2\beta}{64r^6 \pi^3} \\
&+ \frac{\left(\left(\frac{r}{F}\right)^W (W+1)(n^2 - 1 - 2n) - 2n + n^2 \right) \alpha}{(n^2 - 1 - 2n)r^2} \\
&+ \frac{3m(16\pi^2 r^3 - 9m\beta)}{64\pi^3 r^6}, \\
\bar{\rho} + 2\bar{P}_t + \bar{P}_r &= 2 \left(\frac{32r^4 \left(\frac{r}{F}\right)^W W(1+3n+n^2-n^3) - \left(\frac{r}{F}\right)^W (64r^4 n^4 - 128r^4 n^3)}{64r^6(n^2 - 2n - 1)} \alpha \right)
\end{aligned}$$

$$\begin{aligned}
& + \frac{64r^4n^2\left(\frac{r}{F}\right)^W - 64r^4n^4 + 128r^4n^3}{64r^6(n^2 - 2n - 1)}\alpha + \frac{48m\pi^2r^3 - 9m^2\beta}{64r^6\pi^3} \\
& + \frac{\left(\left(\frac{r}{F}\right)^W (1 + W)(n^2 - 2n - 1) - 2n + n^2\right)\alpha}{(n^2 - 1 - 2n)r^2} \\
& - \frac{(1 + 2n)\left(\left(\frac{r}{F}\right)^W (n^2 - 1 - 2n) + n^2 - 2n\right)\alpha}{(n^2 - 2n - 1)r^2} \\
& + \frac{3m(16\pi^2r^3 - 9m\beta)}{64\pi^3r^6} + \frac{48m\pi^2r^3 - 9m^2\beta}{64\pi^3r^6}, \\
\bar{\rho} - \bar{P}_r = & \frac{\left(\left(\frac{r}{F}\right)^W (1 + W)(n^2 - 2n - 1) - 2n + n^2\right)\alpha}{(n^2 - 1 - 2n)r^2} \\
& + \frac{(1 + 2n)\left(\left(\frac{r}{F}\right)^W (n^2 - 1 - 2n) + n^2 - 2n\right)\alpha}{(n^2 - 2n - 1)r^2} \\
& + \frac{3m(16\pi^2r^3 - 9m\beta)}{64\pi^3r^6} - \frac{48m\pi^2r^3 - 9m^2\beta}{64\pi^3r^6}, \\
\bar{\rho} - \bar{P}_t = & - \frac{32r^4\left(\frac{r}{F}\right)^W W(1 + 3n + n^2 - n^3) - \left(\frac{r}{F}\right)^W (64r^4n^4 - 128r^4n^3)}{64r^6(n^2 - 2n - 1)}\alpha \\
& - \frac{64r^4n^2\left(\frac{r}{F}\right)^W - 64r^4n^4 + 128r^4n^3}{64r^6(n^2 - 2n - 1)}\alpha - \frac{48m\pi^2r^3 - 9m^2\beta}{64r^6\pi^3} \\
& + \frac{\left(\left(\frac{r}{F}\right)^W (1 + W)(n^2 - 1 - 2n) - 2n + n^2\right)\alpha}{(n^2 - 1 - 2n)r^2} \\
& + \frac{3m(16\pi^2r^3 - 9m\beta)}{64\pi^3r^6},
\end{aligned}$$

and also corresponding to solution II are

$$\bar{\rho} = \frac{\left(\frac{r}{F}\right)^W (1 + W)(1 + 4n + 3n^2 - 2n^3) - n^2}{(1 + 2n)(n^2 - 2n - 1)r^2}\alpha$$

$$\begin{aligned}
& + \frac{3m(16\pi^2 r^3 - 9m\beta)}{64\pi^3 r^6}, \\
\bar{\rho} + \bar{P}_r &= \frac{\left(\frac{r}{F}\right)^W (1 + 4n + 3n^2 - 2n^3) - n^2}{(n^2 - 2n - 1)r^2} \alpha + \frac{48m\pi^2 r^3 - 9m^2\beta}{64\pi^3 r^6} \\
& + \frac{\left(\frac{r}{F}\right)^W (1 + W)(1 + 4n + 3n^2 - 2n^3) - n^2}{(1 + 2n)(n^2 - 2n - 1)r^2} \alpha \\
& + \frac{3m(16\pi^2 r^3 - 9m\beta)}{64\pi^3 r^6}, \\
\bar{\rho} + \bar{P}_t &= -\frac{32r^4(2n^2 + 8n^3 + 6n^4 - 4n^5) \left(\frac{r}{F}\right)^W + (1 + 5n + 7n^2) \left(\frac{r}{F}\right)^W W}{64r^6(2n + 1)(n^2 - 2n - 1)} \alpha \\
& + \frac{(n^3 - 2n^4) \left(\frac{r}{F}\right)^W W}{64r^6(1 + 2n)(n^2 - 1 - 2n)} \alpha - \frac{2n^4}{64r^6(1 + 2n)(n^2 - 2n - 1)} \alpha \\
& + \frac{\left(\frac{r}{F}\right)^W (1 + W)(1 + 4n + 3n^2 - 2n^3) - n^2}{(1 + 2n)(n^2 - 2n - 1)r^2} \alpha \\
& + \frac{3m(16\pi^2 r^3 - 9m\beta)}{64\pi^3 r^6} + \frac{48m\pi^2 r^3 - 9m^2\beta}{64r^6\pi^3}, \\
\bar{\rho} + \bar{P}_r + 2\bar{P}_t &= 2 \left(-\frac{32r^4(2n^2 + 8n^3 + 6n^4 - 4n^5) \left(\frac{r}{F}\right)^W + (1 + 5n + 7n^2) \left(\frac{r}{F}\right)^W W}{64r^6(1 + 2n)(n^2 - 2n - 1)} \alpha \right. \\
& + \frac{(n^3 - 2n^4) \left(\frac{r}{F}\right)^W W}{64r^6(1 + 2n)(n^2 - 1 - 2n)} \alpha - \frac{2n^4}{64r^6(1 + 2n)(n^2 - 2n - 1)} \alpha \\
& \left. + \frac{48m\pi^2 r^3 - 9m^2\beta}{64r^6\pi^3} \right) + \frac{\left(\frac{r}{F}\right)^W (1 + W)(1 + 4n + 3n^2 - 2n^3) - n^2}{(1 + 2n)(n^2 - 2n - 1)r^2} \alpha \\
& + \frac{\left(\frac{r}{F}\right)^W (1 + 4n + 3n^2 - 2n^3) - n^2}{(n^2 - 2n - 1)r^2} \alpha + \frac{48m\pi^2 r^3 - 9m^2\beta}{64\pi^3 r^6} \\
& + \frac{3m(16\pi^2 r^3 - 9m\beta)}{64\pi^3 r^6}, \\
\bar{\rho} - \bar{P}_r &= \frac{\left(\frac{r}{F}\right)^W (1 + W)(1 + 4n + 3n^2 - 2n^3) - n^2}{(1 + 2n)(n^2 - 2n - 1)r^2} \alpha + \frac{3m(16\pi^2 r^3 + 15m\beta)}{64\pi^3 r^6} \\
& - \frac{\left(\frac{r}{F}\right)^W (1 + 4n + 3n^2 - 2n^3) - n^2}{(n^2 - 2n - 1)r^2} \alpha - \frac{48m\pi^2 r^3 - 9m^2\beta}{64\pi^3 r^6},
\end{aligned}$$

$$\begin{aligned}
\bar{\rho} - \bar{P}_t &= \frac{32r^4(2n^2 + 8n^3 + 6n^4 - 4n^5) \left(\frac{r}{F}\right)^W + (1 + 5n + 7n^2) \left(\frac{r}{F}\right)^W W}{64r^6(2n + 1)(n^2 - 1 - 2n)} \alpha \\
&- \frac{(n^3 - 2n^4)W \left(\frac{r}{F}\right)^W}{64r^6(1 + 2n)(n^2 - 1 - 2n)} \alpha + \frac{2n^4}{64r^6(1 + 2n)(n^2 - 2n - 1)} \alpha \\
&- \frac{48m\pi^2 r^3 - 9m^2\beta}{64r^6\pi^3} + \frac{3m(16\pi^2 r^3 - 9m\beta)}{64\pi^3 r^6} \\
&+ \frac{\left(\frac{r}{F}\right)^W (1 + W)(1 + 4n + 3n^2 - 2n^3) - n^2}{(1 + 2n)(n^2 - 2n - 1)r^2} \alpha.
\end{aligned}$$

These conditions become corresponding to solution III as

$$\begin{aligned}
\bar{\rho} &= \frac{48m\pi^2 r^3 - 8(1 + 2n)\pi^2 r^{4+2n} A\alpha - 27m^2\beta}{64\pi^3 r^6}, \\
\bar{\rho} + \bar{P}_r &= \frac{48m\pi^2 r^3 - 8(1 + 2n)\pi^2 r^{4+2n} A\alpha - 27m^2\beta}{64\pi^3 r^6} \\
&+ \frac{48m\pi^2 r^3 + 8(1 + 2n)\pi^2 r^{4+2n} A\alpha - 9m^2\beta}{64\pi^3 r^6}, \\
\bar{\rho} + \bar{P}_t &= \frac{48m\pi^2 r^3 - 8(1 + 2n)\pi^2 r^{4+2n} A\alpha - 27m^2\beta}{64\pi^3 r^6} \\
&+ \frac{48m\pi^2 r^3 + 8n(1 + 2n)\pi^2 r^{4+2n} A\alpha - 9m^2\beta}{64\pi^3 r^6}, \\
\bar{\rho} + \bar{P}_r + 2\bar{P}_t &= \frac{48m\pi^2 r^3 - 8(1 + 2n)\pi^2 r^{4+2n} A\alpha - 27m^2\beta}{64\pi^3 r^6} \\
&+ \frac{48m\pi^2 r^3 + 8(1 + 2n)\pi^2 r^{4+2n} A\alpha - 9m^2\beta}{64\pi^3 r^6} \\
&+ 2\left(\frac{48m\pi^2 r^3 + 8n(1 + 2n)\pi^2 r^{4+2n} A\alpha - 9m^2\beta}{64\pi^3 r^6}\right), \\
\bar{\rho} - \bar{P}_r &= \frac{48m\pi^2 r^3 - 8(1 + 2n)\pi^2 r^{4+2n} A\alpha - 27m^2\beta}{64\pi^3 r^6} \\
&- \frac{48m\pi^2 r^3 + 8(1 + 2n)\pi^2 r^{4+2n} A\alpha - 9m^2\beta}{64\pi^3 r^6}, \\
\bar{\rho} - \bar{P}_t &= \frac{48m\pi^2 r^3 - 8(1 + 2n)\pi^2 r^{4+2n} A\alpha - 27m^2\beta}{64\pi^3 r^6} \\
&- \frac{48m\pi^2 r^3 + 8n(1 + 2n)\pi^2 r^{4+2n} A\alpha - 9m^2\beta}{64\pi^3 r^6}.
\end{aligned}$$

References

- [1] Herrera, L.: Phys. Lett. A **165**(1992)206.
- [2] Ruderman, M.: Ann. Rev. Astron. Astrophys. **10**(1972)427.
- [3] Mak, M.K. and Harko, T.: Int. J. Mod. Phys. D **13**(2004)149.
- [4] Gleiser, M. and Dev, K.: Int. J. Mod. Phys. D **13**(2004)1389.
- [5] Sharma, R. and Maharaj, S.D.: Mon. Not. R. Astron. Soc. **375**(2007)1265.
- [6] Rahaman, F. et al.: Astrophys. Space Sci. **330**(2010)249.
- [7] Kalam, M. et al.: Eur. Phys. J. C **73**(2013)2409.
- [8] Bhar, P. et al.: Eur. Phys. J. C **75**(2015)190.
- [9] Maurya, S.K., Gupta, Y.K. and Ray, S.: Eur. Phys. J. C **77**(2017)36.
- [10] Ovalle, J.: Mod. Phys. Lett. A **23**(2008)3247.
- [11] Ovalle, J.: Phys. Rev. D **95**(2017)104019.
- [12] Ovalle, J. et al.: Eur. Phys. J. C **78**(2018)960.
- [13] Gabbanelli, L., Rincon, A. and Rubio, C.: Eur. Phys. J. C **78**(2018)370.
- [14] Graterol, R.P.: Eur. Phys. J. C **133**(2018)244.
- [15] Sharif, M. and Sadiq, S.: Eur. Phys. J. C **78**(2018)410.
- [16] Morales, E. and Tello-Ortiz, F.: Eur. Phys. J. C **78**(2018)841.
- [17] Maurya, S.K., Banerjee, A. and Hansraj, S.: Phys. Rev. D **97**(2018)044022.
- [18] Hensh, S. and Stuchlík, Z.: Eur. Phys. J. C **79**(2019)834.
- [19] Casadio, R. et al.: Eur. Phys. J. C **79**(2019)826.
- [20] Sharif, M. and Sadiq, S.: Int. J. Mod. Phys. D **28**(2019)2040004.

- [21] Zubair, M. and Azmat, H.: Ann. Phys. **420**(2020)168248.
- [22] Rincón, Á. et al.: Eur. Phys. J. C **80**(2020)1.
- [23] Contreras, E., Tello-Ortiz, F. and Maurya, S.K.: Class. Quantum Grav. **37**(2020)155002.
- [24] Contreras, E., Ovalle, J. and Casadio, R.: Phys. Rev. D **103**(2021)044020.
- [25] Carrasco-Hidalgo, M. and Contreras, E.: Eur. Phys. J. C **81**(2021)757.
- [26] Buchdahl, H.A.: Mon. Not. R. Astron. Soc. **150**(1970)1.
- [27] Harko, T., Koivisto, T.S. and Lobo, F.S.N.: Mod. Phys. Lett. A **26**(2011)1467.
- [28] Harko, T. et al.: Phys. Rev. D **84**(2011)024020.
- [29] Haghani, Z. et al.: Phys. Rev. D **88**(2013)044023.
- [30] Sharif, M. and Waseem, A.: Chin. J. Phys. **60**(2019)26.
- [31] Sharif, M. and Waseem, A.: Ann. Phys. **405**(2019)14.
- [32] Maurya, S.K. et al.: Phys. Dark Universe **30**(2020)100640.
- [33] Maurya, S.K. and Tello-Ortiz, F.: Phys. Dark Universe **27**(2020)100442.
- [34] Zubair, M. and Azmat, H.: Eur. Phys. J. Plus **136**(2021)112.
- [35] Muneer, Q., Zubair, M. and Rahseed, M.: Phys. Scr. **96**(2021)125015.
- [36] Maurya, S.K., Tello-Ortiz, F. and Ray, S.: Phys. Dark Universe **31**(2021)100753.
- [37] Azmat, H., Zubair, M. and Ahmad, Z.: Ann. Phys. **439**(2022)168769.
- [38] Sharif, M. and Naseer, T.: Chin. J. Phys. **73**(2021)179; Indian J. Phys. (to appear, 2022) arXiv:2203.03268v1.
- [39] Naseer, T. and Sharif, M.: Universe **8**(2022)62.
- [40] Katirci, N. and Kavuk, M.: Eur. Phys. J. Plus **129**(2014)163.

- [41] Faraji, M., Rashidi, N. and Nozari, K.: arXiv:2107.13547v1.
- [42] Sharif, M. and Naz, S.: Universe **8**(2022)142.
- [43] Board, C.V.R. and Barrow, J.D.: Phys. Rev. D **96**(2017)123517.
- [44] Nari, N. and Roshan, M.: Phys. Rev. D **98**(2018)024031.
- [45] Akarsu, Ö. et al.: Phys. Rev. D **97**(2018)124017.
- [46] Bahamonde, S., Marciu, M. and Rudra, P.: Phys. Rev. D **100**(2019)083511.
- [47] Barbar, A.H., Awad, A.M. and AlFiky, M.T.: Phys. Rev. D **101**(2020)044058.
- [48] Sharif, M. and Gul, M.Z.: Phys. Scr. **96**(2020)025002; Eur. Phys. J **136**(2021)1; Int. J. Mod. Phys. A **36**(2021)2150004; Mod. Phys. Lett. A **37**(2022)2250005; Int. J. Geom. Methods Mod. Phys. **19**(2022)2250012.
- [49] Sharif, M. and Naz, S.: Eur. Phys. J. Plus **137**(2022)421; Int. J. Mod. Phys. D (to appear 2022); Mod. Phys. Lett. A (to appear, 2022).
- [50] Brown, J. D.: Class. Quantum Grav. **10**(1993)1579; Seliger, R. L. and Whitham, G.B.: Proc. R. Soc. **305**(1968)1.
- [51] Avelino, P.P. and Sousa, L.: Phys. Rev. D **97**(2018)064019.
- [52] Mendoza, S. and Silva, S.: Int. J. Geom. Methods Mod. Phys. **18**(2021)2150059.
- [53] Maurya, S.K. et al.: Phys. Rev. D **100**(2019)044014.
- [54] Sharif, M. and Furqan, F.: Indian J. Phys. (to appear, 2022).
- [55] Tolman, R.C.: Phys. Rev. **55**(1939)364.
- [56] Darmonis, G.: Memorial des Sciences Mathematiques (Gauthier-Villars, 1927).
- [57] Sharif, M. and Majid, A.: Phys. Dark Universe **30**(2020)100610; Chin. J. Phys **68**(2020)406.

- [58] Abreu, H., Hernandez, H. and Nunez, L.A.: *Class. Quantum Grav.* **24**(2007)4631.
- [59] Herrera, L.: *Phys. Lett. A* **165**(1992)206.
- [60] Buchdahl, H.A.: *Phys. Rev. D* **116**(1959)1027.
- [61] Bowers, R.L. and Liang, E.P.T.: *Astrophys. J.* **188**(1974)657.